euronoise

Frequency and phase characteristics of the edge tone

György Paál and István Vaik

Budapest University of Technology and Economics, P. O. Box 91, 1521 Budapest, Hungary
paal@hds.bme.hu

Extensive experimental and computational work was performed to characterize the edge tone phenomenon. The dependence of the oscillating frequency on some of the main parameters of the configuration including the nozzle-wedge distance and the mean velocity magnitude and profile shape of the jet was measured. The frequency was obtained from the FFT of a pressure sensor signal. The measured and computed frequencies are compared and show a very good agreement.
For both the CFD simulations and the experiments the phase of the oscillation and the pressure at specified points on the wedge are correlated. For the experiments the phase of the flow oscillation is determined with the help of flow visualization pictures obtained by a high speed digital camera.

1 Introduction

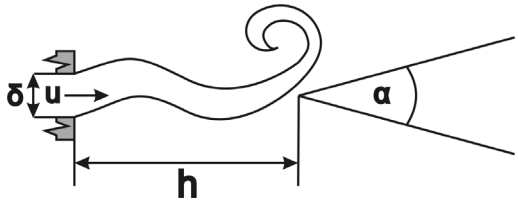

Figure 1. Sketch of the edge tone configuration

The edge tone is a simple flow configuration producing a remarkably complex behavior. It consists of a plane jet and a wedge-shaped object, opposite of the jet exit (Figure 1.). It was observed that the jet oscillates around the wedge (also called edge) in a more or less periodic manner [1-5]. Under certain conditions the configuration can emit an audible tone at the oscillation frequency. The aim of this work is to describe the rig and the methods, wherewith these frequencies can be measured as accurately as the available measurement instruments and the uncertainty of the process itself allow. The relationship between the Strouhal number and the Reynolds number can be determined, based on the experimental data. Finally, this can be compared with the results of CFX simulations, partially published before [6].

2 Experimental system and instrumentation

The rig to produce the edge tone flow is depicted in Fig.1a. Shop air with a pressure reduced to 0.5 bar was led by ¾" reinforced flexible plastic tubes to a cylindrical pressure reservoir with a volume of 57 l. A mass flow rate sensor (Sensortechnics, Honeywell AWM700, working on a heated element principle with a voltage output) was built into the line between the pressure reducing valve and the reservoir tank to determine the mean velocity of the jet. The sensor was also placed between two throttle valves to keep the pressure at the sensor constant. (Fig. 2a) This was required because it was found during the sensor calibration that the output signal is very sensitive to the pressure at the sensor. There is also a long straight copper pipe section before the sensor to ensure undisturbed inflow.

Two different nozzles were used to create a top hat or a parabolic velocity profile for the jet. For the top hat profile the nozzle was formed by two quarter-cylinders leading to a quick contraction (Fig. 2b). The dimensions of this nozzle were 3.4 and 76 mm, respectively, yielding an aspect ratio of over 22. This ensured good two-dimensionality in the central region. The nozzle to create a jet with parabolic velocity profile had an orifice with dimensions of 2.9 mm and 64.3 mmcorresponding to an aspect ratio of 22 again. Before the orifice two parallel 55 mm long plates ensured the development of the parabolic velocity profile. (Fig. 2c)

The wedge was made of well-polished solid steel with an angle of $\alpha = 30°$. Its height (z direction) was 150 mm i. e. this dimension was twice as long as the slit of the nozzle to avoid end effects. Also the x-dimension of wedge was much longer compared with experimental setups reported elsewhere in the literature. The distance between the nozzle

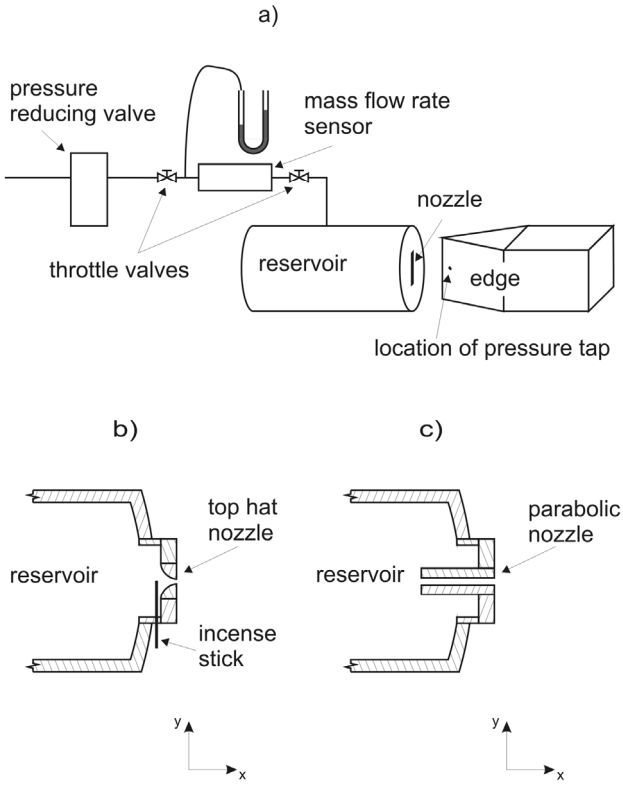

Figure 2. a) Sketch of the measurement system; b) Details of the top hat nozzle; c) Details of the parabolic nozzle

and the wedge is adjustable in the range of 5 to 53 mm. A pressure transducer (Sensortechnics, 113LP01D-PCB) was built into the wedge to measure the surface pressure at a distance of 26.2 mm from the tip of the wedge. The measuring range of this sensor is [-100 Pa; 100 Pa] and the output for this range is [1 V; 6 V]. The pressure amplitude for the lower range of Reynolds numbers is less than 10 Pa so that the output signal of the pressure transducer was in the range of [3.25 V; 3.75V]. In order to be able to digitalize this (or even smaller) pressures with the 12 bit National Instruments A/D converter card the analogue signal of the pressure transducer was amplified with a special amplifier. This way the [3.25 V; 3.75 V] voltage

region could be extended to the [0 V; 10 V] region. When using the nozzle creating a top hat profile jet the flow can be visualized with an incense stick inserted just before the nozzle confusor. The smoke filament is illuminated with floodlight and the image was recorded with a high speed digital camera (LaVision ImagerCompact) taking pictures with a maximum frequency of 90 Hz with a spatial resolution of 320x240 pixels. No visualization was made in the parabolic case.

Each instrument was carefully calibrated before carrying out the measurements. The flow rate sensor was calibrated using an inverted bell which sinks while squeezing out air at a uniform rate. The sinking speed is then proportional with the flow rate. It was discovered here that the output signal is sensitive to the pressure at the sensor so that the pressure was kept constant there. The output signal was proportional with the supply voltage so that the supply voltage was also kept constant. Further details are omitted here. The pressure transducer was calibrated with the help of a micromanometer for the full range and the behaviour was found perfectly linear. For the relevant ±5 Pa range no separate calibration was made in the absence of a suitable device. However, the linearity and the frequency independence of the amplifier was checked and found satisfactory.

3 Measurement procedure

To be able to compare the results of the measurements with the CFD results of the authors non-dimensional frequency values are needed. The non-dimensionalised velocity (Reynolds number) and frequency (Strouhal number) were defined as follows:

$$\mathrm{Re} = \frac{u\delta}{v} \text{ and } St = \frac{f\delta}{u}$$

where u is the mean exit velocity of the jet, δ is the width of the slit of the nozzle, v is the kinematic viscosity of the air, and f is the frequency of jet oscillation.

The uncertainty in the measured Reynolds number based on the error in the factors composing it was about 1.5 %.

Data were obtained at different Reynolds numbers at different nozzle-wedge distances with different jet velocity profiles. Initially four methods were used to determine the oscillation frequency:

1) FFT of the time history of the pressure signal
2) Processing the photo-series taken of the smoke filament

a. – "Vortex counting method"
b.– "wavelength method"

3) Stroboscope principle

3.1 Frequency from the pressure signal

The amplified output voltage of the pressure transducer was captured for 10-50 seconds depending on the lowest frequency component of the oscillation, with 4-10 kHz sampling frequency depending on the highest frequency component of the oscillation. The captured data was processed by LabView code. Data processing includes FFT and plotting the pressure history and its spectra as well as data saving. The signal to noise ratio is usually quite low. Further data processing covers the smoothing of the signal to make it more suitable for synchronizing the pressure and the photos taken of the oscillating jet. The grey graph in Figure 3a represents the recorded while the black one the smoothed data. In Figure 3b the spectrum in the frequency range of interest belonging to Figure 3a is presented. The error in the Strouhal number obtained with this method was typically around 4%.

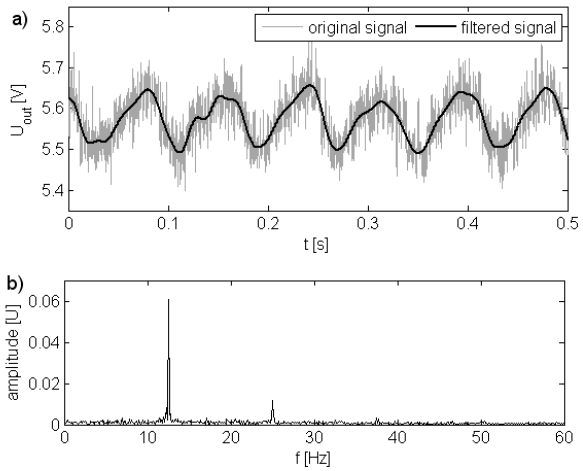

Figure 3. a) pressure history unfiltered (grey) and filtered (black); b) Spectrum belonging to a). Re = 250

3.2 Frequency from image processing

a) One of the methods is to count the visualized vortices passing at a fixed spatial point next to the wedge and measuring the time between two passages. Since the error in the measurement of time is negligible the error of this measurement is at most half a vortex, resulting in an error in the Strouhal number of 3.5%. (The detailed analysis is omitted here.)

b) The other method estimates the disturbance wavelength visually and measures the disturbance propagation speed by comparing the position of the constant phase point in two subsequent images. These positions can be queried by the software of the camera. From the images the half wavelength could be measured easily, since in most of the cases it was not possible to observe a full wave. The wavelength is defined as double of the half wavelength. This method has a significantly larger error, resulting in errors in the Strouhal numbers in the order of 15-30%.

The method has another principal weakness; it was assumed that the wavelength and the speed of disturbance propagation are independent of phase and spatial location. This assumption was demonstrated to be wrong as by the computations in [6].

Both techniques based on processing of the photo-series are only capable of determining the oscillation frequency of the highest stage (see next chapter). When there is a second stage oscillation with the first stage present it is impossible to measure the frequency of the first stage with these methods.

3.3 Frequency by stroboscope

A fourth method of measuring the oscillation frequency is simply to use a stroboscope light. This could be used only for low Reynolds numbers since with the appearance of higher modes the periodicity disappears. The error is estimated to be 4%.

4 Results and discussion

4.1 Comparison of the various methods

First, the above-mentioned frequency measuring methods are compared. Figure 4. shows the comparison for the first stage.

The measurement methods compare very well; they all agree within their accuracy.

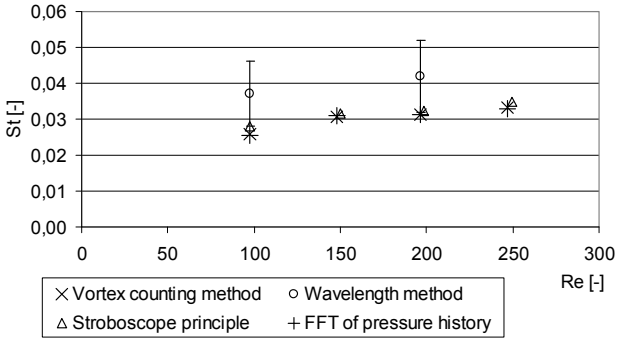

Figure 4. Comparison of the Strouhal numbers measured with different methods. Stage I., top hat profile, h/δ = 10

This is valid even for the "wavelength method", which has a much larger error than the rest of the methods.

From this point onwards only the pressure transducer method will be used since it is the fastest and most flexible method, and that is the only one which is capable of capturing several stages simultaneously with good accuracy. In the case of the parabolic velocity profile, only this method has been used.

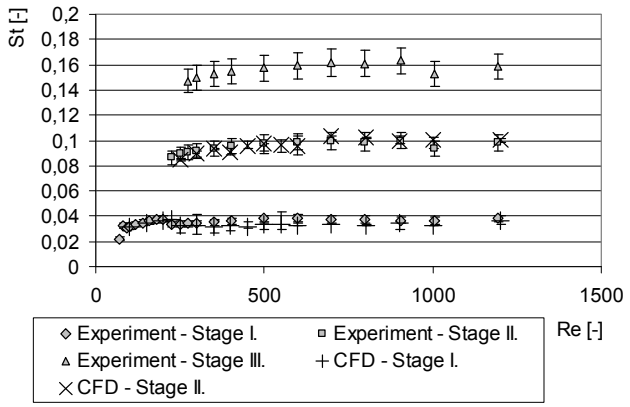

Figure 5. Reynolds number dependence of the Strouhal number; top hat profile, h/δ = 10;

4.2 Comparison of experiments and simulations

First we keep the nozzle – wedge tip distance constant and vary the Reynolds number. The results are presented in Figure 5.

Generally we can state that the agreement between measurements and CFD simulations is excellent. The first oscillation was observed at around Re = 70 and this event is captured equally well with both methods. At around Re ≈ 220 the second stage appears, without the disappearance of the first stage. Again this point is predicted with CFD almost exactly at the right place, as well as the fact that the two stages coexist. At the point of the appearance of the second stage a slight drop of the Strouhal number of the first stage can be observed, again, both in the computations and in the measurements. The reason for this could be that the two modes of oscillation interact. The third stage in the experiments appears surprisingly early, at around Re ≈ 275. In the computations the third stage appears much later at about Re = 1400. The upper limit for the Reynolds number in the measurements was constrained by the calibration of the mass flow rate sensor.

Next the Reynolds number is kept constant and the nozzle – wedge tip distance is varied. It is well accepted in the literature that the relationship between the Strouhal number and the nozzle-wedge distance number follows the relationship:

$$St \propto \frac{1}{\left(h/\delta\right)^n}$$

There are differences in the value of n, varying between 1 [1, 7] and 1.5 [8, 9]. The results confirm convincingly that the n = 1 dependence gives a very good fit for all three stages, similarly to the computational results of [6]. (Due to the lack of space not all the results can be presented here)

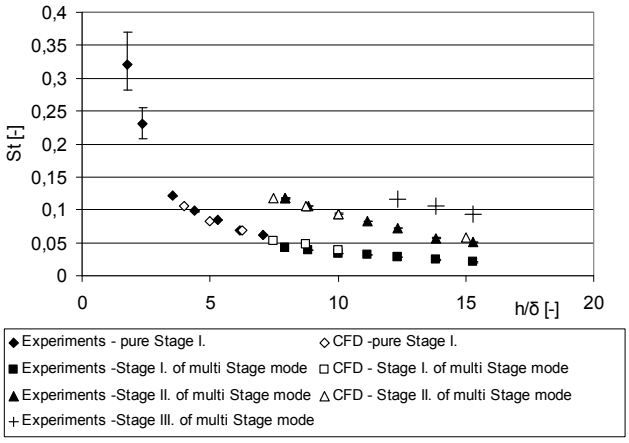

Figure 6. Nozzle-wedge distance dependence of the Strouhal number; Comparison of experimental and CFD results; Re = 350, top hat profile

In Figure 6. comparison between measurements and simulations for the nozzle – wedge tip dependence is presented. The agreement is again excellent, except for the inception of oscillation and which both happens earlier in the experiments than in the simulations. The third stage was not found in the simulations. Figure 7. shows comparisons

for the parabolic profile for constant distance, varying Reynolds number. The agreement is still good, although a little less so than in the top hat profile case. Here, however, there is a fundamental difference. In the case of the experiments, the lower stage exists further after the appearance of the higher stage, similarly to the top hat profile case. In the case of the computations, however, the lower stage disappears soon after the higher stage has appeared. The literature confirms the computational findings [10] so that we do not want to make a judgement at the moment for the reasons of the disagreement. For example, we have no means to check whether the velocity profile in the experiments is really parabolic.

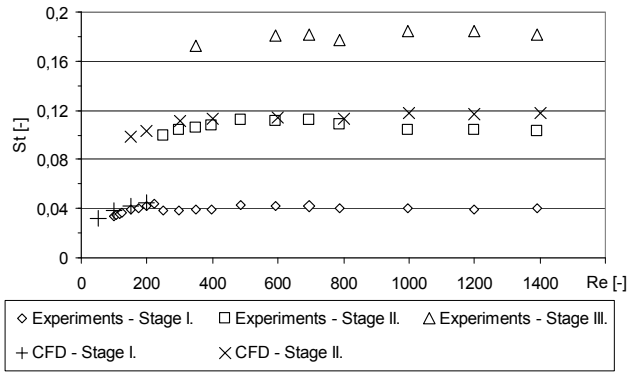

Figure 7. Reynolds number dependence of the Strouhal number; h/δ = 10, parabolic profile

A similar inverse dependence from the nozzle – wedge tip distance for the parabolic profile as for the top hat profile is confirmed (not shown here).

4.3 Relation of phase and jet position

Figure 8a and b show the relationship of the jet shape and the phase of the pressure signal determined experimentally and computationally. The virtual smoke was a passive scalar emitted in the central third of the nozzle. The minimum pressure on the lower side is reached when the jet is in the top extreme position and maximum pressure when it is in the bottom position. The zero crossings correspond roughly to the medium positions of the jet. It is interesting to observe that the pressure signal in the experiments is not perfectly periodic; there is a variation from period to period. In the computations where there is much less noise the signal is naturally more periodic. The smaller indentation in the computational pressure signal presumably corresponds to the passage of the secondary vortex along the pressure tap.

5 Conclusion

It was demonstrated that four different measurement methods to determine the edge tone oscillation frequency agreed very well. The pressure transducer method was chosen for detailed measurements and the results were compared with computational results for both the top hat and the parabolic exit velocity profile. The agreement was excellent everywhere, except that the third stage appeared at lower Reynolds numbers in the experiments and in some cases the lower limit of the oscillation was lower in the experiments.

Correlation was set up between the jet position and the phase of the pressure signal and again good agreement was found between the computations and the experiments.

Acknowledgements

This work has been supported by the Hungarian National Fund for Science and Research under contract Nr. OTKA T46304.

References

[1] Brown, G. B., 1937, „ The vortex motion causing edge tones” *Proc. Phys. Soc. Lond.* Vol. 49., pp. 493-507

[2] Jones, A. T., 1942., “Edge tones”, *J. Acoust. Soc. Am.*, Vol. 14, pp. 131-139.

[3] Nyborg, W. L., Burkhard, M. D. and Schilling, H. K., 1952, “Acoustical characteristics of jet-edge and jet-edge-resonator systems” *J. Acoust. Soc. Am.*, Vol. 24, pp. 293-304

[4] Curle, N., 1953, “The mechanics of edge tones”. *Proc. Roy. Soc.* A. Vol. 216, pp 412-424

[5] Powell, A., 1961, “On the edge tone”, *J. Acoust. Soc. Am.*, Vol. 33, pp. 395-409.

[6] G. Paál, I. Vaik, 2007 Unsteady flow phenomena in the edge tone, *Int. J. Heat Fluid Flow*, Vol. 28, pp. 575-586

[7] Bamberger, A., Baensch, E., Siebert, K., 2004, "Experimental and numerical investigation of edge tones", *Z. Angew. Math.* 84. Nr. 6, pp. 1-15

[8] Crighton D., 1992, “The edgetone feedback cycle. Linear theory for the operating stages”, *J. Fluid Mech.*, Vol. 234, pp. 361-391.

[9] Holger, D., Wilson, T. and Beavers G., 1977, “Fluid mechanics of the edgetone”, *J. Acoust. Soc. Am.*, Vol. 62, pp. 1116-1128.

[10] Ségoufin, C., Fabre, B. and de Lacombe, L., 2004, “Experimental investigation of the flue channel geometry influence on edge tone oscillations”, *Acta Acustica united with Acusica*, Vol. 90, pp. 966-975

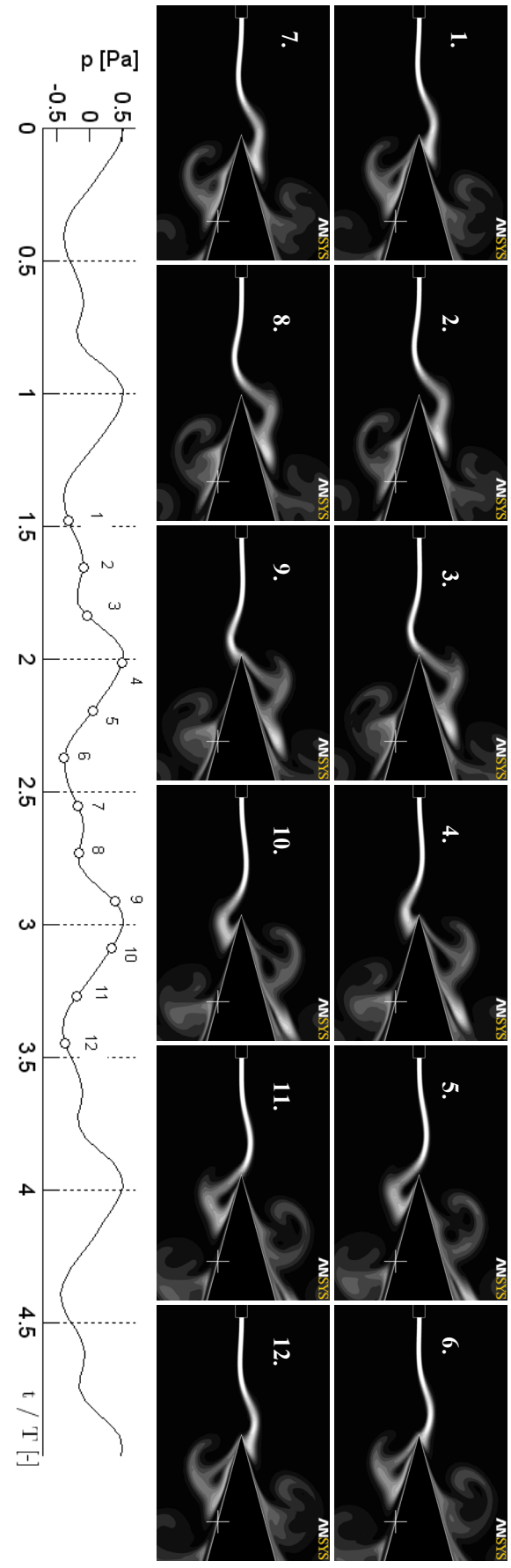

Figure 8b. Two periods of computational visualisation of a first stage oscillation, and the pressure signal at the point indicated by the white cross; Re = 200

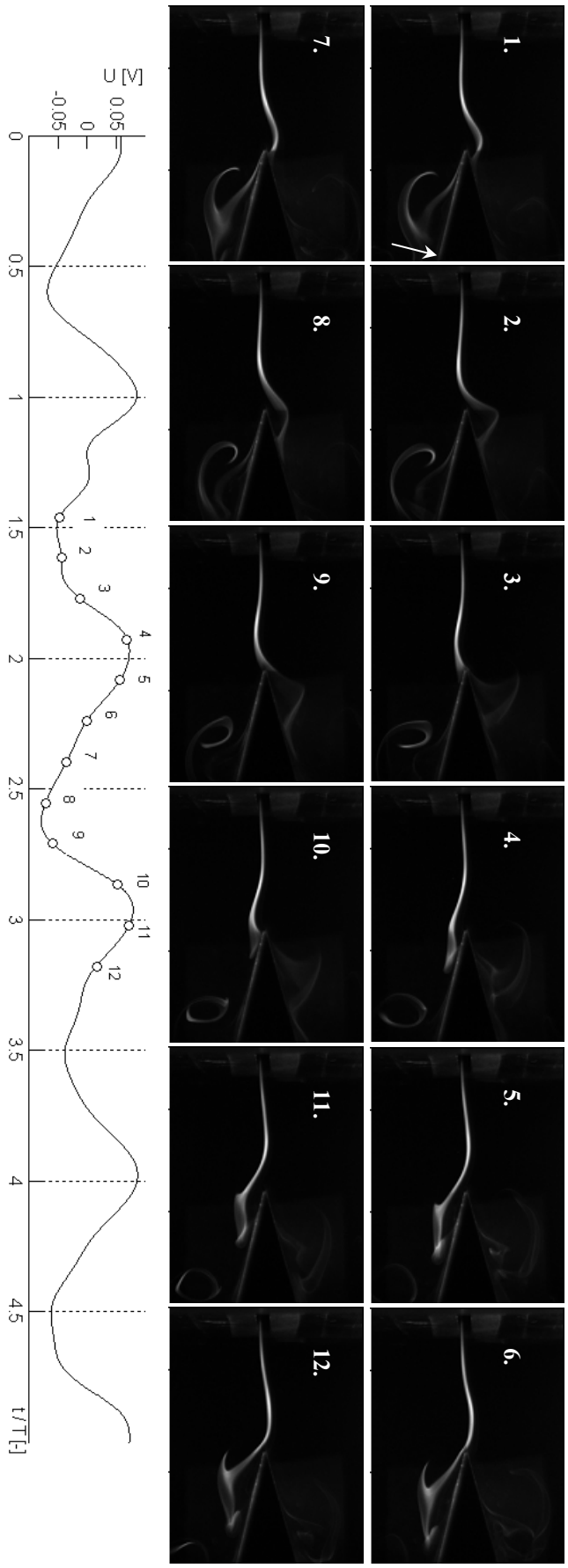

Figure 8a. Two periods of smoke visualisation of a first stage oscillation took at 80 fps, and the filtered output signal of the pressure sensor;
Re = 250; location of pressure tap is indicated by the white arrow in Frame 1